BIOCHEMISTRY
including biophysical chemistry & molecular biology
Article

Biochemistry **2010,** *49,* 4827–4832 4827
DOI: 10.1021/bi100478j

Role of Aggregation in Rhodopsin Signal Transduction†

Marilisa Neri, Stefano Vanni, Ivano Tavernelli, and Ursula Rothlisberger*

Laboratory of Computational Chemistry, Ecole Polytechnique Fédérale de Lausanne, Lausanne CH-1015, Switzerland

Received March 31, 2010; Revised Manuscript Received May 7, 2010

ABSTRACT: Many G protein-coupled receptors (GPCRs) are known to form dimers or even oligomers, and these aggregated states have been proposed as functional units responsible for signal transduction and G protein activation. However, the nature of their involvement has remained elusive. Here, we have investigated the role of aggregation in the signal transduction for dimeric forms of the prototypical GPCR rhodopsin using molecular dynamics simulations. The early steps after photoexcitation are characterized by a tandem mechanism in which one monomer is responsible for light detection while the other serves as the G protein activation site. Dimerization ensures efficient cross-talk between the two units within a few tens of nanoseconds following photoexcitation. This interface-mediated pathway suggests oligomerization-aided signal transduction as a crucial biological strategy to enhance activation efficiency across the entire family of GPCRs.

G protein-coupled receptors (GPCRs)[1] are a large class of transmembrane proteins that respond to a wide range of extracellular stimuli, including light, hormones, neurotransmitters, biogenetic amines, and odorants, and thus constitute central components of a variety of biological signal transduction pathways (*1*). Despite a low degree of sequence identity, GPCRs share a highly homologous fold characterized by the presence of seven transmembrane helices, and all mediate extracellular signals into the cell (*1*). Within the GPCR family, rhodopsin is responsible for light detection and represents a prototypical system to understand the mechanism of GPCR signaling (*2*). In the dark state, the binding site is occupied by the inverse agonist 11-*cis* retinal, which is covalently linked to residue K296 of transmembrane helix 7 (TM7) via a protonated Schiff base. Photoinduced isomerization of the chromophore from 11-*cis* to all-*trans* inside the binding pocket leads to a cascade of conformational changes that take place on the millisecond time scale, ultimately leading to receptor activation and downstream signaling. A number of distinct intermediates of the photocycle have been detected: photorhodopsin (occurring ca. 200 fs after photoisomerization), batho (picoseconds), blue-shifted intermediate (BSI) and lumi (nanoseconds), meta-I (microseconds), and meta-II (milliseconds), the active conformation for G protein coupling (*3*). Some structural features of the very early intermediates have been elucidated by experimental data (*4*−*6*) and molecular dynamics simulations (MD) (*7*−*9*), which show that the main strain of the retinal after isomerization is released through a swinging motion of the β-ionone ring (*10*). Several experimental studies revealed that the activated state meta-II is characterized by the outward movement of the cytoplasmic end of TM6 and TM5 relative to TM3 (*11*−*13*), a feature that has also been observed in the recent crystal structure of opsin (*14*) bound to a G protein fragment. This movement is considered to be one of the hallmarks of the transition to the active state leading to the opening of a cleft in the cytoplasmic domain of rhodopsin that is part of the G protein-binding site.

In contrast, much less information is available on the mechanistic details of the signal transduction at the molecular level. The most acknowledged activation mechanisms involve the breakage of a salt bridge (ionic lock) between R135 of the D(E)RY motif of TM3 and E247 in the cytoplasmatic end of TM6 accompanying rearrangements in the regions of the conserved $NPxxY(x)_{5,6}F$ motif and/or a conformational transition of W265 of the CWxP motif in TM6, the so-called rotamer toggle switch (*11*, *13*−*18*).

The picture is further complicated by the fact that several studies reveal that GPCRs are organized as oligomers (*19*−*25*), suggesting aggregated states might be involved in the activation of rhodopsin and/or its binding to the G protein transducin (*26*). Albeit monomers are capable of activating transducin, dimeric forms have been shown to couple the G protein more efficiently (*27*, *28*); however, this issue remains somewhat controversial (*26*, *29*). This raises the fundamental question about the possible role of oligomerization in signal transduction and in the molecular mechanisms of GPCR activation. In fact, since GPCRs are important drug targets in the treatment of many diseases, further elucidation of the specificity and physiological significance of GPCR dimerization may lead to insights that could impact the development of future therapeutics (*30*).

To explore the role of dimerization for activation and signal transduction, we performed several explicit membrane MD simulations of a rhodopsin dimer. All simulations are based on the atomic force microscopy data of the rhodopsin dimer in its native disk membrane (*19*, *20*) where the dimer interface involves TM4, TM5, and also part of TM3 and intracellular loop 2 (IL2) connecting TM3 and TM4, in agreement with cross-linking studies of the dopamine D2 receptor and other experimental findings (*24*, *31*, *32*) and with recent interesting computationl work on GPCR dimerization (*26*). Using MD simulations, we followed the signal transduction upon photoisomerization up to the microsecond time range. These studies reveal that the activation process occurs in an asymmetric fashion: photoexcitation of

†Financial support for these studies was provided by Swiss National Science Foundation Grant 200020-116294.

*To whom correspondence should be addressed. E-mail: ursula.roethlisberger@epfl.ch. Phone: +41 21 69 30321,30325. Fax: +41 (0)21 693 03 20.

[1]Abbreviations: GPCR, G protein-coupled receptor; BSI, blue-shifted intermediate; MD, molecular dynamics; IL, intracellular loop; TM, transmembrane helix.

Published on Web 05/11/2010

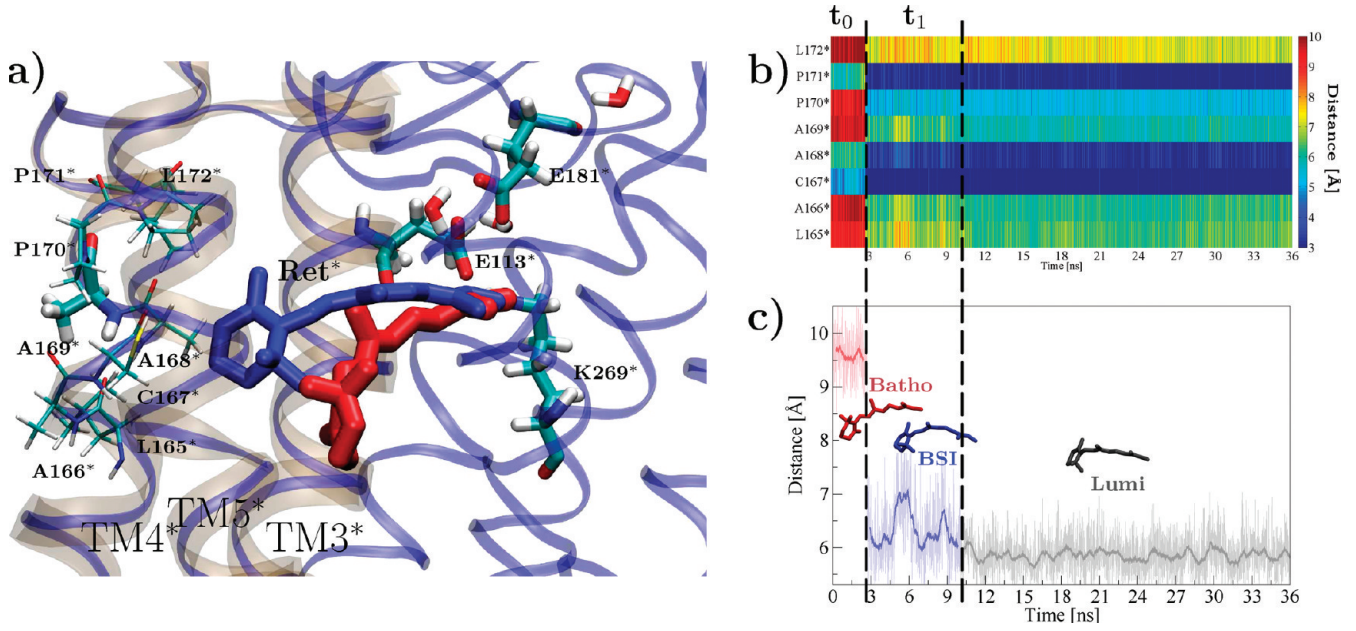

FIGURE 1: (a) Localization of the retinal inside the binding pocket in the batho (red licorice) and BSI (blue licorice) states. Residues belonging to TM4* (from L165* to L172*) as well as the counterions E113*, E181*, and K296* and internal water molecules are also depicted. (b) Minimum distance between the ionone ring and the residues forming the binding pocket in TM4* as a function of time, color coded according to the scale indicated on the right. (c) Time evolution of the minimal distance between the ionone ring and A169*. Different colors identify the different conformations of the chromophore in the photoactivated Rho* subunit: red represents the batho state, blue BSI, and gray lumi.

the chromophore in one monomer (Rho*) induces conformational changes in the other monomer (Rho), where the "ionic lock" breaks triggering evolution toward the meta-II state (*14*).

MATERIALS AND METHODS

Molecular System. A 7 ns equilibrated structure of the rhodopsin monomer (*7*) was used to build up the rhodopsin dimer so as to reproduce the protein−protein interface observed in the hexameric model of the recent atomic force microscopy model (PBD code 1N3M) (*19*). All possibly charged amino acids were considered charged except D83 and E122 (*7*). All histidine residues present in the protein are assumed to be protonated either in the N_δ position (H100, H211) or in the N_ε position (H65, H152, H195, H278). Two palmitoyl chains bonded to C322 and C323 as membrane anchoring points were included in both of the subunits. The system has been immersed in a preequilibrated explicit membrane mimicked by 1-stearoyl-2-oleoyl-*sn*-glycero-3-phosphoethanolamine (SOPE) lipids and in explicit water in such a way that TM8 lies at the hydrophobic/hydrophilic interface, with the hydrophilic residues pointing toward the aqueous phase. The size of the periodic cubic box is approximately 130 × 80 × 100 Å^3 with ∼20000 water molecules and ∼300 lipids resulting in a total of ∼100000 atoms (see Figure S1). The box dimensions are chosen in such a way that the minimum distance between periodic images of the protein is always larger than 30 Å throughout all simulations.

MD Simulations. We used the SPC (*33*) and AMBER/parm99 (*34*) force fields for water and for the protein dimer, respectively, and for the lipid bilayer the same force field used previously (*35*, *36*). All data collections and equilibration runs were done using GROMACS 4 (*37*). Electrostatic interactions were calculated with the Ewald particle mesh method (*38*), with a real space cutoff of 11 Å. Bonds involving hydrogen atoms were constrained using the LINCS (*39*) algorithm, and the time integration step was set to 2 fs. The system was coupled to a

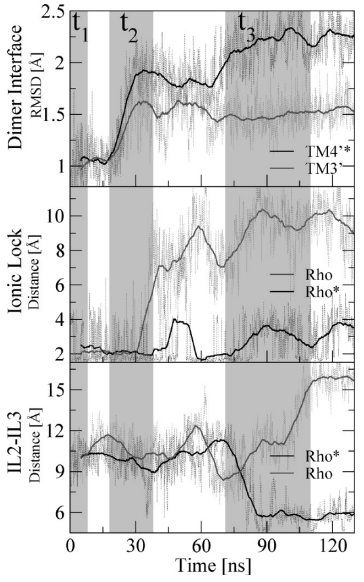

FIGURE 2: Upper panel: Root mean square deviation (rmsd) of the residues in the cytoplasmatic part of TM4* (TM4′*, residues from H152* to V162*) in black and of residues in TM3 (TM3′, from L131 to V139) in gray. Middle panel: Time evolution of the N_η−O_δ distance between R135 and E247 of the ionic lock in Rho (gray line) and Rho* subunit (black). (The complete time evolution of this quantity is depicted in Figure S7.) Lower panel: Time evolution of the distance between the center of mass of the C_α atoms of loops IL2 (IL2*) (from residue C140 to E150) and IL3 (IL3*) (from L226 to A246) in gray (black).

Berendsen bath (*40*) with 0.2 ps relaxation time for the temperature and 1.0 ps for the pressure. All simulations were subjected to periodic boundary condition in the three directions of the Cartesian space. The water/lipid box was equilibrated via 10 ns of MD. After immersion of the dimer and placement of the ions, the box underwent another 5 ns of MD with the protein kept fixed. This was followed by a series of slow annealings to equilibrate the

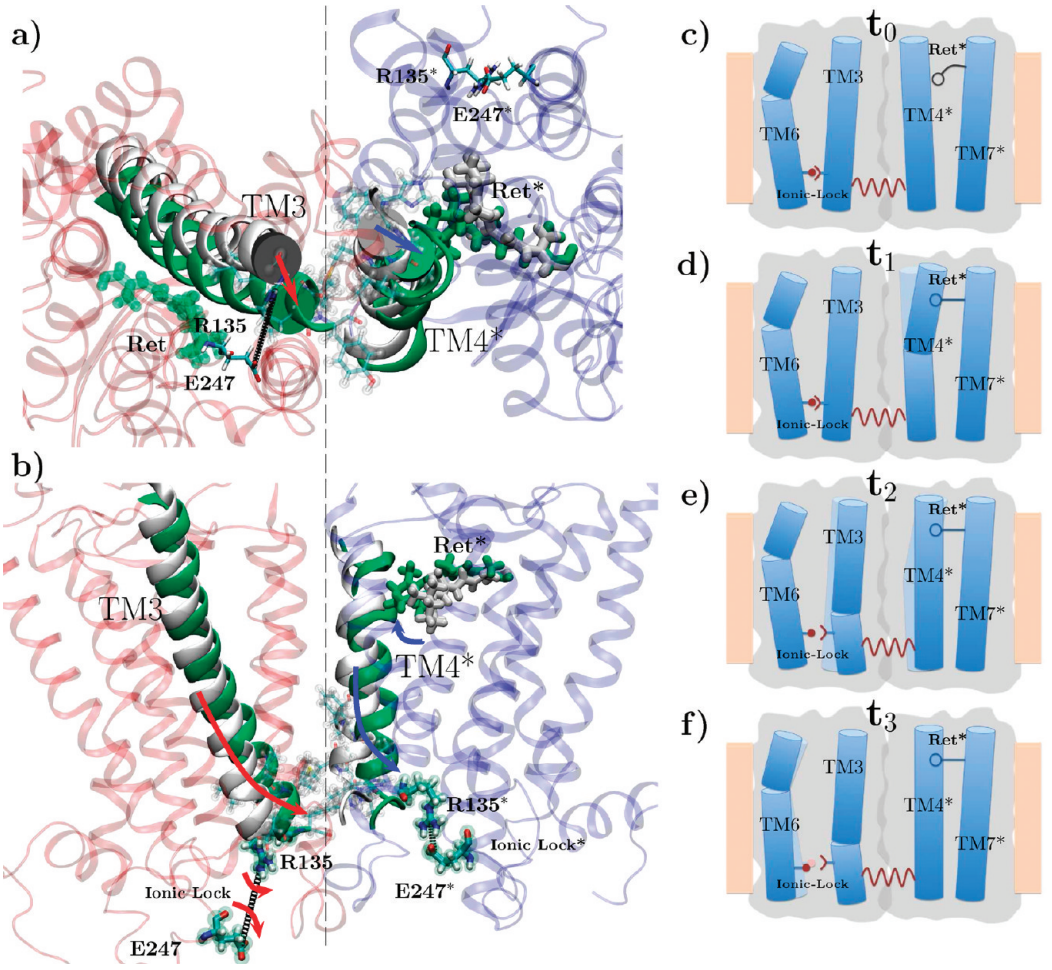

FIGURE 3: Left panel: Bottom (a) and side (b) view of the rhodopsin dimer. Red and blue ribbons refer to Rho and Rho* subunits, respectively. White and green ribbons represent TM3, TM4*, and retinal in time windows t_1 and t_2, respectively. The ionic lock, which is disrupted in Rho and formed in Rho*, is also shown at time window t_2. Right panel: Summary of the main structural changes in schematic cartoon representations in different time windows from t_0 to t_3. In each time window the previous configuration is reported in light blue to highlight the structural changes. (c) Time window t_0: the retinal is in the batho state and the receptor is in the initial rest state. (d) t_1: the retinal is in the BSI/Lumi state and the upper part of TM4* is bent toward the binding pocket of the Rho* subunit. (e) t_2: movement of the cytoplasmatic part of TM4* and TM3 induces ionic lock disruption. (f) t_3: straightening of TM6 eases the opening of the cytoplasmatic cleft in the subunit Rho.

full system. Approximately 300 ns of classical MD of the rhodopsin dimer in the dark state (Rho-Rho system) was performed in the NPT ensemble at a temperature of 310 K and a pressure of 1.05 bar. In the fully equilibrated system the root mean square deviation (rmsd) for the C_α positions is stable at ~2.5 Å with respect to the initial reference coordinates. During the MD simulation of the Rho-Rho system, the quaternary structure of the dimer did not change much from the initial structure, preserving the features of the AFM model (*19*). Specifically, both TM4 helices remain in close contact with the intradiscal segment of TM5 and with the cytoplasmatic end of TM3 of the complementary subunit.

A harmonic restraint was applied to enforce the isomerization process (see Figure S2, top panel) in one subunit of the dimer, Rho*. A harmonic potential with a force constant of 50 kcal mol^{-1} rad^{-2} was applied to the $C_{10}-C_{11}-C_{12}-C_{13}$ torsional angle, changing from −10° to 180° in 2 ps. After the isomerization had occurred, the MD simulations of the rhodopsin dimer system were continued without any restraints. Four MD isomerization attempts were performed starting from different snapshots of the Rho-Rho trajectory (two Rho-Rho* and two Rho*-Rho simulations; see Figure S7). The discussed signal transduction mechanism was confirmed in all four independent simulations (Figure S7).

All data analyses were done using GROMACS (*37*) utilities, and all molecular images were made with visual molecular dynamics (VMD) (*41*).

RESULTS

The primary reaction in the rhodopsin photocycle is the *cis*−*trans* isomerization of the $C_{11}-C_{12}$ double bond of the chromophore occurring in an electronically excited state on the subpicosecond time scale. Applying the same procedure as previously reported (*7*, *8*), we drive the isomerization process in one of the two subunits (Rho*). After inducing isomerization of the retinal, we followed the real time evolution of the system up to microseconds. Starting from different initial conditions, we performed four independent MD simulations, and in all of them we invariably observed an identical signal transduction pathway, which is characterized by three major steps:

Step 1: Early Events in the Signal Transduction Pathway. Up to ~3 ns the retinal-protonated Schiff base (Figure 1a, time windows t_0) is characterized by a high internal strain due to steric repulsion between the C_{19} and C_{20} methyl groups ($\phi_{dihedral}$ ($C_{19}-C_9-C_{13}-C_{20}$) ~ 70°, Figure S2). In agreement with previous experimental findings (*10*) and simulation studies of monomeric rhodopsin (*7*, *8*), this internal strain is released by a

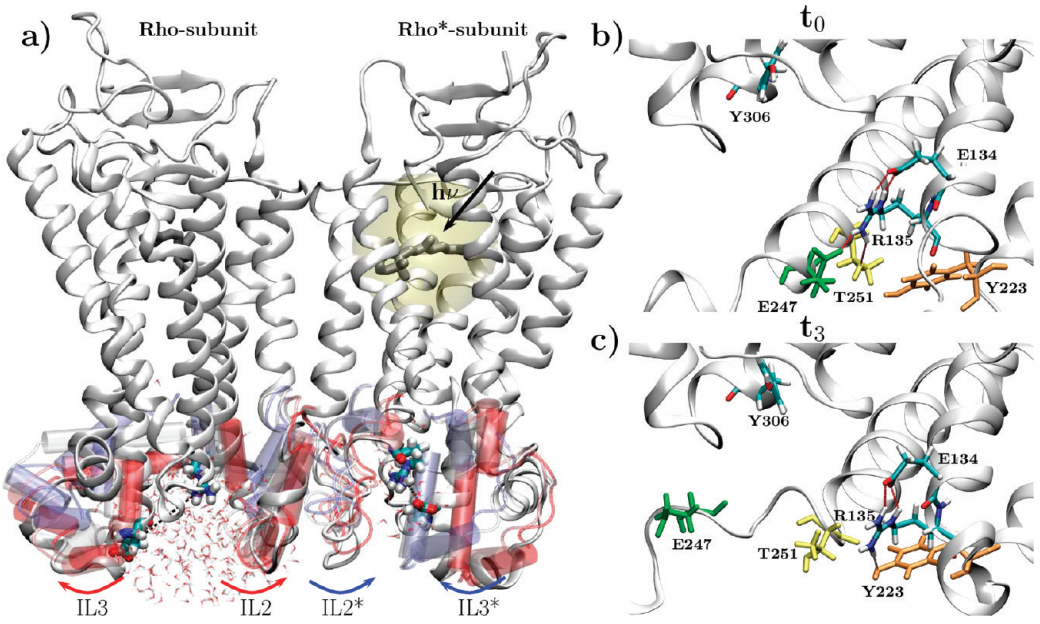

FIGURE 4: (a) Rhodopsin dimer in tube representation (dark white). The gray licorice depicts the chromophore position in Rho*. The ionic lock in both subunits is also shown at time window t_3. The cartoon superimposition of the position of loops IL2 (IL2*) and IL3 (IL3*) as a function of time starting from red (t_0) to blue (t_3) is shown. (b, c) Geometry of the cytoplasmatic part of the subunit Rho in time windows t_0 and t_3, respectively. The residues that undergo the main structural rearrangement are depicted in orange (Y223), green (E247), and yellow (T251) while E134, R135, and Y306 are shown in atom-type color code. The red dashed lines refer to the hydrogen bond interactions.

sudden flip of the ionone ring (Figure 1 and Figure S2a) from its initial location between TM5* and TM6* to a new position flanked by TM4* and TM5* (Figure 1). This movement allows for an essentially planar all-*trans* conformation of the polyene chain (see Figure 1a and Figure S3) and reduces the distance between the ionone ring and A169* in the interfacial TM4* from ca. 10 Å in the dark state to approximately 6 Å. This is in line with cross-linking experiments that identified A169* as the cross-linking partner of the β-ionone ring in later photointermediates, whereas W265* is its preferred partner in the dark state (*10*, *31*, *42*). Further inspection of the time evolution of the distance between the ionone ring and A169* over the entire trajectory of half a microsecond clearly reveals the presence of three distinct intermediates (Figure 1b,c). Preliminary calculations of the corresponding absorption spectra confirm the possible assignment of the first intermediate with batho (around 3 ns after photoisomerization and before the flip of the ionone ring), the second with BSI (after the flip of the ionone ring, around 3−10 ns), and the third with lumi (around 10 ns). These structures of the early intermediates are virtually identical to the ones previously reported for monomer simulations (*7*), and in addition, the structure of batho is in excellent agreement with the available crystallographic data (*5*). Furthermore, we were also able to observe the later intermediate lumi, which differs from BSI by a flip of the torsional angle around the C_2-C_3 bond of the ionone ring (C_2-C_3 = 60° in BSI and C_2-C_3 = −60° in lumi, as shown in Figure S4). These early conformational changes occur within a time window of few nanoseconds (t_1) and trigger the instantaneous transmission of the signal to the binding pocket of the monomer Rho*, as illustrated in Figure 1a,b and Figure S2b. The displacement of A168* and A169* leads to an increased van der Waals interaction between the ionone ring and the extracellular half of TM4* (see Figure S5). As a result, the C-terminal part (residues ranging from M163* to P171*) of TM4* undergoes a bending of ~3° toward the binding pocket, creating a kink in between V162* and M163* (see Figure 3d and Figure S6a).

Step 2: Signal Transduction through the Protein−Protein Interface. The subsequent structural evolution is monitored in Figure 2. The next major conformational changes take place approximately at 30 ns after photoisomerization (Figure 2, time window t_2). Interestingly, this change is located at the dimer interface as shown by the displacement of the cytoplasmatic end of the two interfacial helices TM4* in the photoexcited monomer and TM3 in the dark subunit (Figure 2, top panel, and Figure 3e). The bending of the C-terminal part of TM4* toward the binding pocket is followed by a displacement of the cytoplasmatic end of TM4* toward the same direction, so that TM4* regains a fully extended conformation. These combined movements of the C- and N-terminal halves of TM4* result in its rigid translation away from the dimer interface (see Figure 3a,e and Figure S6a,c).

Via a group of hydrophobic residues (from H152* to V162*), the N-terminal part of TM4* is anchored (see Figure 3 and Figure S6d) to the cytoplasmatic end of TM3 (from L131 to V139). As a result, the displacement of TM4* drags along the C-terminal part of TM3 (Figure 2, top panel, Figure 3, and Figure S6b), causing signal transmission across the dimer interface from the initially photoexcited Rho* subunit to the dark subunit Rho. The tilt of the cytoplasmatic end of TM3 causes breakage of the "ionic lock" between R135 in TM3 and E247 in TM6 in the dark subunit Rho (Figure 2, middle panel, Figure 3a,b, and Figure 4c), a well-known characteristic of rhodopsin activation (*13*).

Our computational experiments thus suggest a tandem mechanism for signal transduction in the rhodopsin dimer in which one monomer serves as light sensor and transmits the signal to the other subunit that gets activated for G protein interaction.

Step 3: Asymmetric Activation of the Rhodopsin Dimer. Further conformational changes arise in time window t_3 around 70 ns (Figure 2, bottom panel). The disruption of the "ionic lock" in the dark subunit Rho increases the mobility of the intracellular end of the protein, that evolves toward an opsin-like active configuration (*14*). In particular, an outward movement of the cytoplasmatic end of TM6 relative to TM3 is observed

(see Figure 3f and Figure S9) and IL2 and IL3 of the dark monomer Rho move apart from each other (Figure 2, bottom panel, and Figure 4a). These rearrangements expose a hydrophobic patch and the conserved E(D)RY motif of Rho to the solvent, providing a potential recognition site for the C-terminus of the α-subunit of transducin (GαCt) (*11*, *13*−*15*, *17*, *18*) (Figure 4c). Simultaneously, IL2* and IL3* move in an anticorrelated fashion, leading to a closure of the cytoplasmatic cleft of the photoactivated unit Rho* (Figure 2, bottom panel, Figure 4a, and Figure S8). Analysis of the covariance matrix (*43*) shows that the closing and opening of the cytoplasmic clefts in Rho* and Rho are concerted. In fact, the movements of IL2 (IL2*) and IL3 (IL3*) are strongly anticorrelated while those of IL2 and IL2* are correlated (Figure S8).

As a consequence of the outward movement of TM6, the interactions between the side chains of E247 and T251 with R135 are broken and replaced by a newly formed hydrogen bond with the hydroxyl group of Y223 in TM5 (see Figure 4b,c). These structural changes in the proximity of R135 closely reproduce the active-like features revealed in the crystal structure of opsin (*14*). Further conformational changes involving the interaction between R135 and E134 as well as the movement of Y306 are likely to occur upon protonation of E134 in later stages of the activation process (*17*, *44*).

DISCUSSION

In conclusion, these results provide a picture of the structural changes involved in the early signal transduction pathway in rhodopsin. We were able to identify three main steps in the activation mechanism. The first one involves the switch of the ionone ring in the photoisomerized subunit Rho*, which initiates the signaling cascade via a bending of the extracellular part of TM4* toward the binding pocket of subunit Rho* (*10*, *31*, *42*). In the second step, the signal is further transmitted to the cytoplasmatic part of TM4* coupled to a rearrangement of TM3, causing the disruption of the "ionic lock" in the dark subunit Rho. Finally, in the third step the motions are transmitted to the cytoplasmic loops connecting TM3−TM6, leading to exposure of the E(D)RY motif crucial for G-protein binding.

It turns out that the dimer interface plays a crucial role in this process, mediating the signal from one monomer to the other within a few tens of nanoseconds following photoexcitation. Through an asymmetric mechanism, the relaxation of the photoexcited chromophore in one monomer is directly relayed to the other subunit, where the "ionic lock" breaks and the G protein-binding site undergoes conformational rearrangements toward the active state. This tandem mechanism rationalizes the experimentally observed enhanced activation efficiency for dimeric rhodopsin (*27*, *28*). In fact, the dimer pathway turns out to be more efficient compared to direct activation of the photoactivated monomer, since breakage of the ionic lock in photoactivated subunit Rho* was never observed in any of our simulations. The same holds for simulations at similar length of a single photoactivated monomer. It is therefore evident that monomeric and dimeric forms make use of different activation pathways which could constitute a possible regulatory mechanism for adaptive light detection.

ACKNOWLEDGMENT

We acknowledge Ute Rohrig and Geoffrey Wood for useful discussions.

SUPPORTING INFORMATION AVAILABLE

Figure S1, setup of the rhodopsin dimer system; Figure S2, retinal dynamics; Figure S3, superimposition of the early intermediates of the retinal; Figure S4, transition from BSI to lumi; Figure S5, energy interaction between the retinal and TM4*; Figure S6, conformational changes affecting TM4* and TM3; Figure S7, time evolution of the ionic lock; Figure S8, covariance matrix analysis; Figure S9, superimposition of the opsin structure and subunits Rho and Rho* in time window t_3; coordinates of the dimer model in the dark state as a gromacs format (gro file). This material is available free of charge via the Internet at http://pubs.acs.org.

REFERENCES

1. Pierce, K. L., Premont, R. T., and Lefkowitz, R. J. (2002) Seven-transmembrane receptors. *Nat. Rev. Mol. Cell Biol. 3*, 639–650.
2. Palczewski, K., Kumasaka, T., Hori, T., Behke, A., Motoshima, H., Fox, B. A., Trong, I. L., Teller, D. C., Okada, T., Stenkamp, R. E., Yamamoto, M., and Miyano, M. (2000) Crystal structure of rhodopsin: A G protein-coupled receptor. *Science 289*, 739–745.
3. Schwartz, T. H., Frimurer, T. M., Holst, B., Rosenkilde, M. M., and Elling, C. E. (2006) Molecular mechanism of 7TM receptor activation—a global toggle switch model. *Annu. Rev. Pharmacol. Toxicol. 46*, 481–519.
4. Kukura, P., McCamant, D. W., Yoon, S., Wandschneider, D. B., and Mathies, R. A. (2005) Structural observation of the primary isomerization in vision with femtosecond-stimulated raman. *Science 310*, 1006–1009.
5. Nakamichi, H., and Okada, T. (2006) Crystallographic analysis of primary visual photochemistry. *Angew. Chem., Int. Ed. Engl. 45*, 4270.
6. Salom, D., Lodowski, D. T., Stenkamp, R. E., Golczak, I. L. T. M., Jastrzebska, B., Harris, T., Ballesteros, J. A., and Palczewski, K. (2006) Crystal structure of a photoactivated deprotonated intermediate of rhodopsin. *Proc. Natl. Acad. Sci. U.S.A. 103*, 16123–16128.
7. Rohrig, U. F., Guidoni, L., and Rothlisberger, U. (2002) Early steps of the intramolecular signal transduction in rhodopsin explored by molecular dynamics simulations. *Biochemistry 41*, 10799–10809.
8. Saam, J., Tajkhorshid, E., Hayashi, S., and Schulten, K. (2002) Molecular dynamics investigation of primary photoinduced events in the activation of rhodopsin. *Biophys. J. 83*, 3097–3112.
9. Rohrig, U. F., Guidoni, L., Laio, A., Frank, I., and Rothlisberger, U. (2004) A molecular spring for vision. *J. Am. Chem. Soc. 126*, 15328–15329.
10. Borhan, B., Souto, M. L., Imai, H., Shichida, Y., and Nakanishi, K. (2000) Movement of retinal along the visual transduction path. *Science 288*, 2209–2212.
11. Farrens, D. L., Altenbach, C., Yang, K., Hubbell, W., and Khorana, H. G. (1996) Requirement of rigid-body motion of transmembrane helices for light activation of rhodopsin. *Science 276*, 768–770.
12. Patel, A. B., Crocker, E., Eilers, M., Hirshfeld, A., Sheves, M., and Smith, S. O. (2004) Coupling of retinal isomerization to the activation of rhodopsin. *Proc. Natl. Acad. Sci. U.S.A. 101*, 10048–10053.
13. Altenbach, C., Kusnetzow, A. K., Ernst, O. P., Hofmann, K. P., and Hubbell, W. L. (2008) High-resolution distance mapping in rhodopsin reveals the pattern of helix movement due to activation. *Proc. Natl. Acad. Sci. U.S.A. 105*, 7439–7444.
14. Scheerer, P., Park, J. H., Hildebrand, P. W., Kim, Y. J., Kraub, N., Choe, H., Hofmann, K. P., and Ernst, O. P. (2008) Crystal structure of opsin in its G-protein-interacting conformation. *Nature 455*, 497–502.
15. Franke, R. R., Konig, B., Sakmar, T. P., Khorana, H. G., and Hofmann, K. P. (1990) Rhodopsin mutants that bind but fail to activate transducin. *Science 250*, 123–125.
16. Fritze, O., Filipek, S., Kuksa, V., Palczewski, K., Hofmann, K. P., and Ernst, O. P. (2003) Role of the conserved NPxxY(x)5,6f motif in the rhodopsin ground state and during activation. *Proc. Natl. Acad. Sci. U.S.A. 100*, 2290–2295.
17. Knierim, B., Hofmann, K. P., Ernst, O. P., and Hubbell, W. L. (2007) Sequence of late molecular events in the activation of rhodopsin. *Proc. Natl. Acad. Sci. U.S.A. 104*, 20290–20295.
18. Scheerer, P., Heck, M., Goede, A., Park, J. H., Choe, H., Ernst, O. P., Hofmann, K. P., and Hildebrand, P. W. (2009) Structural and kinetic modeling of an activating helix switch in the rhodopsin-transducin interface. *Proc. Natl. Acad. Sci. U.S.A. 106*, 10660–10665.

19. Liang, Y., Fotiadis, D., Filipek, S., Saperstein, D. A., Palczewski, K., and Engel, A. (2003) Organization of the G protein-coupled receptors rhodopsin and opsin in native membranes. *J. Biol. Chem. 278*, 21655–21662.
20. Fotiadis, D., Liang, Y., Filipek, S., Saperstein, D. A., Palczewski, K., and Engel, A. (2003) Atomic-force microscopy: Rhodopsin dimers in native disc membranes. *Nature 421*, 127–128.
21. Waldhoer, M., Fong, J., Jones, R. M., Lunzer, M. M., Sharma, S. K., Kostenis, E., Portoghese, P. S., and Whistler, J. L. (2005) A heterodimer-selective agonist shows in vivo relevance of G protein-coupled receptor dimers. *Proc. Natl. Acad. Sci. U.S.A. 102*, 9050–9055.
22. Fotiadis, D., Jastrzebska, B., Philippsen, A., and Muller, D. J. (2006) Structure of the rhodopsin dimer: a working model for G-protein-coupled receptors. *Curr. Opin. Struct. Biol. 16*, 252–259.
23. Palczewski, K. (2006) G protein-coupled receptor rhodopsin. *Annu. Rev. Biochem. 75*, 74–7673.
24. Kota, P., Reeves, P. J., Rajbhandary, U. L., and Khorana, H. G. (2006) Opsin is present as dimers in cos1 cells: Identification of amino acids at the dimeric interface. *Proc. Natl. Acad. Sci. U.S.A. 103*, 3054–3059.
25. Lohse, M. J. (2010) Dimerization in GPCR mobility and signaling. *Curr. Opin. Pharmacol. 10*, 53–58.
26. Simpson, L. M., Taddese, B., Wall, I. D., and Reynolds, C. A. (2010) Bioinformatics and molecular modelling approaches to gpcr oligomerization. *Curr. Opin. Pharmacol. 10*, 30–37.
27. Jastrzebska, B., Maeda, T., Zhu, L., Fotiadis, D., Filipek, S., Engel, A., Stenkamp, R. E., and Palczewski, K. (2004) Functional characterization of rhodopsin monomers and dimers in detergents. *J. Biol. Chem. 279*, 54663–54675.
28. Jastrzebska, B., Fotiadis, D., Jang, G., Stenkamp, R. E., Engel, A., and Palczewski, K. (2006) Functional and structural characterization of rhodopsin oligomers. *J. Biol. Chem. 281*, 11917–11922.
29. Whorton, M. R., Bokoch, M. P., Rasmussen, S. G., Huang, B., Zare, R. N., Kobilka, B., and Sunahara, R. K. (2007) A monomeric G protein-coupled receptor isolated in a high-density lipoprotein particle efficiently activates its G protein. *Proc. Natl. Acad. Sci. U.S.A. 104*, 7682–7687.
30. Milligan, G. (2006) G-protein-coupled receptor heterodimers: Pharmacology, function and relevance to drug discovery. *Drug Discov. Today 11*, 541–549.
31. Guo, W., Shi, L., Filizola, M., Weinstein, H., and Javitch, J. A. (2005) Crosstalk in G protein-coupled receptors: Changes at the transmembrane homodimer interface determine activation. *Proc. Natl. Acad. Sci. U.S.A. 102*, 17495–17500.
32. Guo, W., Shi, L., and Javitch, J. A. (2003) The fourth transmembrane segment forms the interface of the dopamine D2 receptor homodimer. *J. Biol. Chem. 278*, 4385–4388.
33. Berendsen, H. J. C., Postma, J. P. M., van Gunsteren, W. F., and Hermans, J. (1981) in Intermolecular Forces (Pullman, B., Ed.) pp 331−342, Reidel, Dordrecht.
34. Cornell, W. D., Cieplak, P., Bayly, C. I., Gould, I. R., Merz, K. M., Ferguson, D. M., Spellmeyer, D. C., Fox, T., Caldwell, J. W., and Kollman, P. A. (1995) A second generation force field for the simulation of proteins, nucleic acids, and organic molecules. *J. Am. Chem. Soc. 117*, 5179–5191.
35. Vanni, S., Neri, M., Tavernelli, I., and Rothlisberger, U. (2010) A conserved protonationinduced switch can trigger ionic-lock formation in adrenergic receptors. *J. Mol. Biol. 397*, 1339–1349.
36. Vanni, S., Neri, M., Tavernelli, I., and Rothlisberger, U. (2009) Observation of ionic lock formation in molecular dynamics simulations of wild-type beta 1 and beta 2 adrenergic receptors. *Biochemistry 48*, 4789–4797.
37. Van der Spoel, D., Lindahl, E., Hess, B., Groenhof, G., Mark, A. E., and Berendsen, H. J. C. (2005) Gromacs: Fast, flexible and free. *J. Comput. Chem. 26*, 1701–1718.
38. Essmann, U., Perera, L., Berkowitz, M. L., Darden, T., Lee, H., and Pedersen, L. G. (1995) A smooth particle mesh Ewald method. *J. Chem. Phys. 103*, 8577–8593.
39. Hess, B., Bekker, H., Berendsen, H. J. C., and Fraaije, J. G. E. M. (1997) Lincs: A linear constraint solver for molecular simulations. *J. Comput. Chem. 18*, 1463–1472.
40. Berendsen, H. J. C., Postma, J. P. M., van Gunsteren, W. F., DiNola, A., and Haak, J. R. (1984) Molecular dynamics with coupling to an external bath. *J. Chem. Phys. 81*, 3684.
41. Humphrey, W., Dalke, A., and Schulten, K. (1996) Vmd—visual molecular dynamics. *J. Mol. Graphics 14*, 33.
42. Furutani, Y., Kandori, H., and Shichida, Y. (2003) Structural changes of water molecules during the photoactivation processes in bovine rhodopsin. *Biochemistry 42*, 9619–9625.
43. Amadei, A., Linssen, A. B., and Berendsen, H. J. (1993) Essential dynamics of proteins. *Proteins 17*, 412–425.
44. Arnis, S., and Hofmann., k. P. (1993) Two different forms of metarhodopsin II: Schiff base deprotonation precedes proton uptake and signaling state. *Proc. Natl. Acad. Sci. U.S.A. 90*, 7849–7853.